JOURNAL OF MATERIALS SCIENCE 23 (1988) 25–34

Impact of substrate materials on the processing and properties of melt-spun nickel-metalloid ribbons

R. P. I. ADLER*, S. C. HSU
GTE Laboratories Incorporated, Waltham, Massachusetts 02254, USA

The dynamic phenomenology of melt spinning with four different nickel-metalloid alloys on copper, molybdenum, aluminium, and iron wheels as well as nickel- and chromium-plated copper substrates has been evaluated. Puddle dimensions are self-adjusting so that the integrated heat flux through the puddle/substrate contact area is sufficient to convert the melt into foil at the same mass flow rate. The dynamic wetting phenomena are complex because mechanical forces dominate during the initial liquid spreading stage, and the solidification process is highly influenced by the melt/substrate interface conditions. Melt spinning does not automatically produce thin section foils with uniform through thickness microstructure. While structural uniformity frequently occurs with "easy" glass-forming alloys, lower metalloid content alloys often develop graded through-thickness microstructures. When this occurs, the degree of crystallinity in the contact surface layer is frequently greater than in the opposite free surface layer.

1. Introduction

Driven by scientific interest and the technological promise of rapid solidification processing (RSP), there has been a substantial annual growth in publications about the processing or properties of RS forms and particulates from a large number of research laboratories [1, 2]. Already a number of US, European and Japanese firms have reduced promise to commercial practice by using improved atomization or melt-spinning techniques. In many cases single roller chill block melt spinning (CBMS) is the preferred variant because it is a high productivity process that is capable of producing nearly 100% yields of a product with a major degree of microstructural refinement and the associated macrochemical uniformity that is unobtainable by conventional metal forming processes.

Encouraged by supplemental research funding from the Office of Naval Research [3, 4], a systematic examination of the critical materials combinations and processing conditions that affect single roller CBMS was undertaken to further implement the rate of technology transfer from the laboratory bench to the factory floor. The overall phenomenologically based approach was to correlate quantitative measurements of melt puddle dynamics and the associated characteristics of continuously solidified ribbon products with materials combinations and processing conditions. Previously some relations between process variables and product characteristics/dimensions [2, 5–16] were empirically established, but fewer correlations of puddle of dynamics and features with product dimensions and quality were published [8, 10, 11, 17, 18].

One phase of our study was to understand the influence of chill block substrate material on the processing and product characteristics. A useful initial overview of this aspect of melt spinning was obtained by assembling a representative listing of the types of substrate materials used to produce various generalized alloy categories of melt-spun product (Table I) from the open patent and publication literature. Not surprisingly, copper, with its excellent heat transfer/capacity properties combined with its reasonable purchase and fabrication costs, appears most frequently. Also, the use of iron-base wheels for melt spinning some iron- or nickel-base products should be noted. In some cases its use is directly recommended over copper or strongly implied when iron-base materials are the only wheel compositions specified in the operating process description. Table II clearly shows that the substantial reduction in the thermal properties relative to copper must be otherwise compensated for by some other beneficial chemical or mechanical effects that were not elaborated on by those workers [21, 23, 25–28].

In examining the basic elements of CBMS, it becomes obvious that there are many parameters that must be closely controlled and monitored if a valid set of experimental observations is to be made. First, there must be a consistent and uniform rate for delivering molten metal into the spatially stationary melt reservoir that rests on the rotating heat-absorbing substrate surface. Also, a stable processing operation will not occur unless this incoming liquid mass flow rate is balanced by the equivalent exiting mass flow rate for the solidified ribbon. Thus, for acceptable high process yields, the primary heat and mass transfer phenomena of a given facility must have sufficient capacity to convert all incoming melt into a continuously

* *Present address*: Army Materials Technology Laboratory, Watertown, Massachusetts 02171, USA.

0022–2461/88 $03.00 + .12

TABLE I Matrix array of substrate materials used to melt spin various categories of alloy foils (references given in brackets)

General Melt Composition	Substrate Material								
	Iron-base			Copper-base					
	Lo carbon	Lo alloy	Stainless	OFHC	Alloy	Ni	Cr	Mo	Al
Ni-base									
(a) Metalloid	[9, 16, 24]*	[16]	[24]	[9, 12, 15, 16, 19, 20, 24]*	[9, 12, 16, 19]	*	*	*	*
(b) Super-alloy	[25†, 26, 28]	[27]		[46]					
(c) Alloy				[24]					
Fe-base									
(a) Metalloid	[9, 16, 24]	[16]	[24]	[9, 11, 12, 15, 16, 19, 20, 24, 29, 30–32]	[9, 12, 16, 19 29]		[11, 29]		
(b) Alloy	[21†, 23]	[21†]	[21†, 22]	[21, 22]					[21]
Cu-base									
(a) Shape memory	[33]		[33]	[29, 33]	[33]				
(b) Alloy	[33]		[33]	[29, 33]	[33]				
(c) (Zr, Ti)-glass	[9]			[9]	[9]				
Al-base				[13, 29, 34]					
Co-base				[30–32, 46]					
Pb-base				[13]					
$Pd_{80}Si_{20}$	[28]			[29]					
Ti-base				[35–37]				[36]	
Rare earth-Fe hard magnet				[38]			[39]		
Mo-base				[40]					

*Present study.
†Author recommends this substrate over copper.

solidified product. Note also that liquid momentum forces (influenced by intrinsic, thermally sensitive melt and substrate surface tension forces and fluid viscosities) have an important effect on the physical spreading of the incoming liquid and its dynamical thermal contact with the rapidly translating substrate. Major elements that influence the magnitude of the melt-to-substrate heat transfer process are: (1) the nature and uniformity of the melt/substrate interface; (2) the magnitude of the intrinsic heat absorption and thermal diffusivity properties of the substrate and any intermediate solidified product materials; and (3) the processing system's capacity to maintain as low as possible effective surface temperature for the substrate. All phenomena that can produce localized perturbations or even systematic effects that cause long-term changes in heat transfer rates will alter the continuous dynamic solidification process and the corresponding dimensions and quality of the product.

Thus, it is experimentally imperative that sufficient quantities of melt be delivered with a constant rate to an internally water-cooled substrate wheel (which is also continuously surface dressed) if unambiguous observations of real differences in steady-state behaviour between various substrate materials are to be separated from transient phenomena. Accordingly, the methodology of this melt-spinning research was to systematically evaluate puddle dynamics and the corresponding product characteristics from initiation to steady-state conditions in order to provide useful substrate selection guidelines for melt-spinning process optimization.

TABLE II Thermal and physical properties of substrates

Material	Melting point (°C)	Properties relative to copper		
		Surface energy	Heat absorption*	Thermal diffusivity†
Cu	1083	1.0	1.0	1.0
Ni on Cu	1452	1.5	1‡	1‡
Cr on Cu	1875	1.6	1‡	1‡
Al	660	0.62	0.40	0.80
Fe	1536	1.31	0.20	0.19
Mo	2610	2.08	0.20	0.65

*Heat absorption = $K\varrho C_p$.
†Thermal diffusivity = $K/\varrho C_p$ where K is the thermal conductivity, ϱ is the density, C_p is specific heat.
‡Neglect effect of thin electroplated layer on bulk thermal characteristics of copper.

2. Experimental procedures

In order to achieve our goal of effectively identifying which substrate material properties are significant to the melt-spinning process, a well-calibrated facility with one set of standardized experimental conditions was used at GTE Laboratories. The melt delivery subsystem consisted of a sealed quartz pressure vessel having an orifice disc with a 1 mm diameter passage in the bottom. This orifice was located directly above the top dead centre of an internally water-cooled, 20.3 cm diameter, melt-quenching wheel. A fixed orifice-to-substrate distance of 1.35 cm was consistently maintained to facilitate viewing and allow dimensional calibration of the film image.

The melt-spinning procedure consisted of inductively heating a prealloyed charge of at least 100 g under a light flow of forming gas (95% N_2–5% H_2) in the melt delivery vessel. Upon reaching the 100° C superheat (measured with a quartz sheathed thermocouple immersed in the melt), the rotating substrate is brought up to 1500 r.p.m. and then the additional forming gas is quickly admitted to the desired overpressure

level of 1.5 psi (10.33×10^{-3} N mm^{-2}) which forces the melt through the orifice, forming a stable jet in air. The jet flow direction is perpendicular to the outer cylindrical surface of the quenchant wheel, which is continuously dressed by a counter-rotating 500-grit abrasive tape flapper wheel device. On impact the jet spreads and typically forms a human-foot-shaped puddle. The longitudinal side view profile of this unencumbered melt puddle is photographed at 1000 frames per second with a Redlake Hycam high-speed (rotating prism and continuously moving film) motion picture camera.

Each film with over 6000 frames provided a record of puddle dynamics for evaluation. Typically quantified measurements of puddle length and height were made from 100 to 150 systematically chosen frames. Because the puddle was somewhat larger and typically more unstable during the initial substrate revolution than for subsequent rotations, most listed puddle characterization measurements are statistical averages, with the associated two standard deviation values from data taken after the initial substrate rotation but during the first three seconds of operation. During this period the melt mass flow rate and the baseline temperature of the rotating substrate usually stabilize. Most foils were also continuous so that sequential evaluation of foil dimensions, micro/macrostructure, morphology, and weight per unit length, could be made and indexed with the number of wheel rotations after startup.

The substrate materials consisted of our standard OFHC copper wheels as well as substrates made from 1040 low carbon steel, 2024 aluminium alloy, sintered molybdenum, and copper electroplated with either chromium or nickel. This group of structural materials provided an opportunity to examine whether substrate characteristics such as surface energy and heat transfer properties affect this form of dynamic wetting. Comparative values such as two thermal figures of merit and surface energy normalized relative to copper as well as melting points are listed in Table II.

A limited array of commercially available ternary nickel-metalloid brazing alloys, including AMS4779 (with 8.7 at % B and 6.6 at % Si), AMS4778 (with 12.8 at % B and 8.3 at % Si), and a modified, low-boron AMS4778 (i.e. 9.4 at % compared to 12.8 at % B in the regular alloy), were chosen because the two metalloid lean melts form crystalline foils when melt spun with a copper wheel, while higher metalloid melts form amorphous foils. In addition nickel-base AMS4777 (with 14.7 at % B, 7.1 at % Si, 2.7 at % Fe, and 6.7 at % Cr) provided an opportunity to evaluate whether the presence of an element common to both the melt and the surface of the wheel had any significant impact on the dynamic wetting process [41–43] occurring during melt spinning. All of these alloys were prepared according to proprietary procedures at the Wesgo Division of GTE Products Corporation.

3. Results and discussion

Characteristics for the puddle dynamics and process features for each melt-spinning run with various combinations of melt and substrate material are listed in Table III. Puddle length varied by a factor of two, being primarily influenced by the type of substrate material rather than the alloy composition of the melt puddle. The order of plotting data in Fig. 1 started with copper, followed by substrate materials with increasingly greater puddle lengths. This order does not directly correspond with any of the surface energy or thermal figures of merit listed in Table II. Using these concepts directly, it is hard to rationalize why both aluminium and molybdenum substrates produced the longest melt puddles, but this will be subsequently explained.

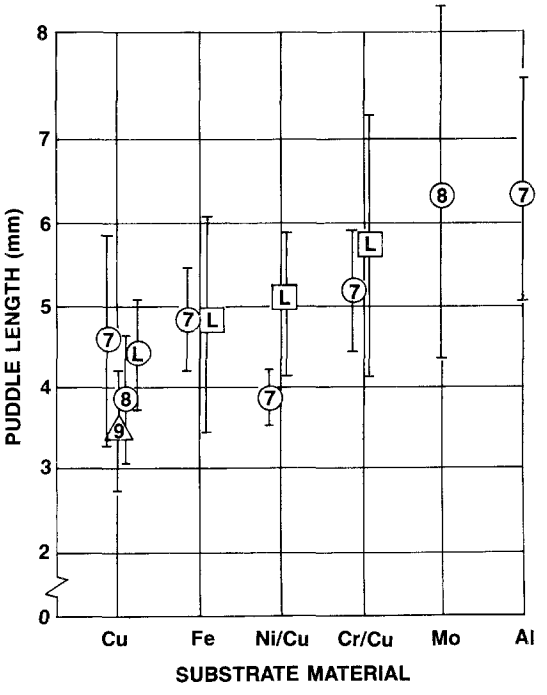

Figure 1 Variation of puddle length for copper and alternate substrate materials. (9) AMS 4779 (crystalline), (8) AMS 4778 (amorphous), (L) lo B AMS 4778 (amorphous), [L] lo B AMS 4778 (crystalline), (7) AMS 4777 (amorphous).

Further interpretation using Table III suggested that the metalloid richer (B > 10 at % and B + Si > 20 at %) alloys (i.e. AMS4777 and 4778) formed larger melt puddles as quantified by the $h \times l$ "area" than the two other alloys with lower metalloid contents. The nominal 20% difference in area was mainly due to the formation of a taller puddle, where side-by-side comparisons will confirm that the higher metalloid puddles have a systematically larger aspect ratio for a given substrate. As all the mass flow rates are comparable, we attribute this to some metalloid-related chemical or physical effect, rather than to some significant changes in the heat or mass transfer mode.

The duration of the foil/wheel contact (or the contact time at 1500 r.p.m.) was measured by observing the circumferential contact arc angle region between the point of jet impingement and that of foil/wheel separation with the aid of a protractor mounted behind the substrate wheel (from the observer). At 1500 r.p.m. each 9° of arc angle represents a 0.001 sec increment in residence time. This arc angle (Table III) can be reasonably correlated with the inverse of the thermal diffusivity figure of merit. One mechanism could be that foil release from the wheel takes place

TABLE III Comparative process values for variable substrate/melt series with similar process conditions*

Parameter	Symbol	Illustration
Puddle length (mm)	$l \pm \Delta l$	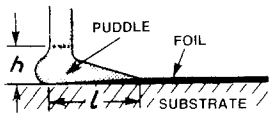
Puddle height (mm)	$h \pm \Delta h$	

Melt	Substrate	Puddle characteristics				Foil/wheel contact (arc angle in degrees)
		Length,† l (mm)	Height,† h (mm)	Aspect ratio, h/l	Area $h \times l$	
AMS4779	Cu	3.47 ± 0.72	2.47 ± 0.80	0.71	8.58	10–15° C (E)
Low B	Cu	4.39 ± 0.66	1.83 ± 0.46	0.42	8.03	25–35°
AMS4778	Fe	4.76 ± 1.30	1.65 ± 0.32	0.35	7.85	25–40° (E)
	Ni/Cu	5.02 ± 0.91	1.57 ± 0.27	0.31	7.86	15°
	Cr/Cu	5.70 ± 1.60	1.51 ± 0.50	0.27	8.59	20°
AMS4778	Cu	3.84 ± 0.79	2.79 ± 0.81	0.73	10.7	25–40° (E)
	Mo	6.31 ± 1.96	1.99 ± 0.78	0.32	12.56	60–90° (E)
AMS4777	Cu	4.62 ± 1.30	2.26 ± 0.70	0.49	10.43	25–30°
	Fe	4.84 ± 0.62	2.35 ± 0.50	0.49	11.35	65°
	Ni/Cu	3.89 ± 0.30	1.78 ± 0.30	0.46	6.92	20–30°
	Cr/Cu	5.16 ± 0.74	1.87 ± 0.38	0.36	9.63	35°
	Al	6.38 ± 1.35	1.84 ± 0.61	0.29	11.74	35°

*Melt ejected through 1 mm diameter orifice with 1.5 psi overpressure onto a substrate wheel rotating at 1500 r.p.m.

†Measured statistics from high speed motion pictures typically over 150 frames; variation range for the mean value from 2σ limits (where σ is the standard deviation) thus only 4.6% of the measurements fall outside of this range.

(E) Estimate only.

after a specific drop in interface temperature downstream of the puddle. Thus substrates with higher thermal diffusivities should have shorter release times. This concept is consistent with our prior experience as well as that of others [12] that wider melt-spun ribbons tend to have longer wheel contact lengths than narrower products. The additional heat release during wider tape melt spinning puts a greater thermal demand on the quenching subsystem. Hence the longer time needed for the surface temperature of the substrate to return to its minimum baseline value effectively increases the contact length during wide foil production.

The increase of the foil/wheel contact length based on common element considerations has been found to be selective rather than universal. For each alloy melt compared to values from a copper wheel (Table III), only iron (in AMS4777) could be shown to increase the contact length on an iron wheel. For chromium (also in AMS4777), a similar extension of the contact length on the chromium-plated wheel was only marginal. In contrast, for all those nickel-base alloys there was no, or even a slightly negative, effect on the contact length when the nickel-plated wheel was used. As this phenomenon empirically appears to be selective, any explicit relationship most probably is masked by other more dominant phenomena.

Characterization of the dimensional values and other foil features for the various combinations of melt and substrate has been summarized in Table IV. Foil widths were measured with a low power filar eyepiece, and the average value for at least 20 readings from a metre-long sample were recorded. Perhaps the most representative and reproducible quantities were the weight per unit length (W/L) data where the specific samples used usually were longer than one metre. Some run-to-run variations in the mass flow rate, as represented by the weight per unit length (W/L) values, are apparent but typically are accommodated by parallel changes in foil width. However, the average calculated thickness (and to a lesser degree, the micrometre-measured thickness values with their inherently larger scatter) remained constant (less than a 10% variation) with time as expected, as substrate rotation rate was already shown to be the dominant parameter controlling foil thickness [4, 44]. This bulk averaged value of the calculated thickness will be used for correlating the systematic, second-order run-to-run variations in puddle dynamics and solidification conditions due to different substrate materials.

Based on one such comparison, the magnitude of the puddle length did not correlate well with the calculated foil thickness which was typically between 3.4 and 3.8. The relative foil thickness growth rates were also calculated from the ratio of foil thickness to the residence time under the puddle. Growth rates ranged from a low of 133 mm sec^{-1} for the AMS4777 melt/aluminium wheel combination, which produced amorphous foil, to a high of 284 mm sec^{-1} for the AMS4779/copper combination, which made fully crystalline foils. Normalized values with respect to the AMS4778/Cu substrate combinations are plotted in Fig. 2. Comparing Figs 1 and 2, the rough inverse trend between puddle length and foil thickening rate indicates that puddle length must be a flexible puddle feature that adjusts to the thermal and mass balance constraints for each operating system.

Although the empirical ranking of the iron wheel

TABLE IV Comparative product values for variable substrate/melt series with similar processing conditions*

Melt	Substrate	Dimensional values				Foil characteristics
		Weight per unit length, W/L ($g\,m^{-1}$)	Width, w (mm)	Thickness, t (mm)	Calculated thickness† ($W/L \div w$)	
AMS 4779	Cu	0.72	2.06	0.062	3.48	Crystalline; minor edge scalloping,‡ longitudinal array of contact surface voids; lightly oxidized free surface.
Low B AMS 4778	Cu	0.75	1.85	0.058	4.04	Amorphous with some fcc phase; good quality with no edge scalloping.
	Fe	0.484	1.21	0.056	3.78	Crystalline; infrequent edge scalloping, contact surface has finer voids often in linear array – may be associated with substrate grooves.
	Ni/Cu	0.504	1.35	0.056	3.77	Crystalline with a trace of amorphous phase; edges with occasional scallop; contact surface is excellent substrate replica with very few voids.
	Cr/Cu	0.455	1.21	0.056	3.60	Crystalline; continuous light scalloped edges, contact surface has random pattern of voids.
AMS 4778	Cu	0.57	1.65	0.056	3.46	Amorphous; infrequent edge scalloping, good quality continuous product.
	Mo	0.73	2.03	0.069	3.82	Amorphous to crystalline – as wheel heats up during run; foils get narrower, more crowned and scalloped.
AMS 4777	Cu	0.674	1.83	0.056	3.71	Amorphous; continuous foil with scalloped edges; free surface protrusions; contact surface has large and small voids.
	Fe	0.505	1.52	0.061	3.45	Amorphous; continuous foil with scalloped and slivered edges; contact surface replicates wheel and has large voids.
	Ni/Cu	0.54	1.40	0.060	3.70	Amorphous; continuous foil with scalloped and slivered edges; contact surface replicates substrate linear features.
	Cr/Cu	0.57	1.78	0.056	3.27	Amorphous; continuous with very heavy edge scalloping; contact surface has large voids.
	Al	0.619	1.75	0.053	3.41	Amorphous; continuous foil with scallops and slivers; contact surface with voids some interconnected.

*Melt ejected through 1 mm orifice with 1.5 psi overpressure onto substrate wheel rotating at 1500 r.p.m.
†Units for calculated thickness values are $10^{-2}\,g\,cm^2$.
‡Scalloped edge features indicative of some transverse puddle surface retraction during melt spinning.

data between those for copper and nickel plated onto copper wheels in Figs 1 and 2 is somewhat subjective, the similarity of the processing characteristics for the iron wheel to both the copper- and the nickel-plated copper wheels was unexpected based on either thermal figure of merit (Table II). Comparative observations of the foil contact surface morphology (Table IV) indicate that the relative melt/substrate intimate contact area for all combinations is typically less than 100%. However, the nickel-plated and the iron wheels seemed to produce foils that had fewer voids and more faithfully replicated the substrate surface finish. At the other extreme the contact surface from foils made from the molybdenum wheel had a larger number of small and large voids [44]; foils made on the aluminium wheel had contact surfaces with extensive, frequently interconnected void patterns that drastically reduced the actual melt/substrate contact area in both cases.

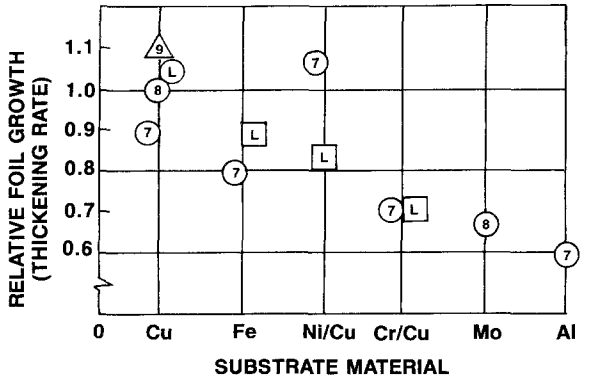

Figure 2 Relative foil thickening rate during solidification under melt puddle for copper and alternate substrate materials. (9) AMS 4779 (crystalline), (8) AMS 4778 (amorphous), (L) lo B AMS 4778 (amorphous), [L] lo B AMS 4778 (crystalline), (7) AMS 4777 (amorphous).

Another probable compounding factor is the presence of a tenacious oxide layer on the chromium and aluminium interfaces that could be expected to further reduce heat transfer rates across the foil/wheel interface in two ways. First, the oxide layer becomes a direct and additional resistive barrier to heat flow. Second, the formation of an oxide reduces the surface energy of the substrate interfaces so that there is an indirect but reduced tendency for the melt to wet uniformly the substrate as effectively [14–43]. Thus both mechanisms can reduce the magnitude of the rapid solidification rate, causing the appropriate puddle length adjustment. Overall for these kinds of

TABLE V X-ray analysis for crystalline/amorphous ratios in low-boron AMS4778 melts spun on various substrates

Run ID and substrate	Sample surface examined*	Peak height (1 1 1) fcc	Integrated area values				Estimated crystallinity from weighted average of $A(1\,1\,1)/2100$ and $A(1\,1\,1)/[A(a) + A(1\,1\,1)]$
			Amorphous hump, $A(a)$	(1 1 1) fcc peak, $A(1\,1\,1)^{\dagger}$	Normalized‡ $A(1\,1\,1)/2100$	$\frac{A(1\,1\,1)}{A(a) + A(1\,1\,1)}$	
2/28/84 Cu	free surface	1130	3700	341	0.162	0.084	~10%
	contact surface	2090	2912	890	0.423	0.234	~25–35%
2/6/84 Fe	free surface	7696	0	2443	≈1	1.0	crystalline
2/7/84 Ni/Cu	free surface	3072	488	1131	0.539	0.699	~70%
2/3/84 Cr/Cu	free surface	4041	0	1851	≈1	1.0	crystalline

*Nominal depth of surface layer sampled by X-radiation was 0.001 cm, based on 95% penetration depth calculations.
†Peak height or area taken above background level or above profile of the broad amorphous hump.
‡For standardized X-ray conditions and uniform irradiated foil area, a fully crystalline AMS4778 foil was arbitrarily assigned a (1 1 1) integrated area intensity value of 2100 counts 2θ (for 2 sec count interval with 0.05° 2θ steps).

nickel-base alloys, copper still appears to be the best substrate material. Even thin electroplated layers of nickel or chromium seem to reduce the thermal transport rate compared to a bare copper quenchant subsystem. The resulting product tends to be narrower and have more pronounced edge scalloping; both are features of partial width reduction of the melt puddle downstream of the impact zone. We [10, 44, 45] have attributed this to a surface tension retraction mechanism that occurs whenever a combination of two conditions exist: (1) the puddle spreading momentum forces decrease to the point where they are no longer dominant; and (2) the extended overlying film of metal is still liquid due to systematically diminished heat transfer rates that in turn reduce the effective rapid solidification rate during melt spinning. When more intimate melt contact was achieved, as in the cases of two melt-spinning runs with an iron wheel and one with the nickel-plated wheel, the effective heat transfer rate was noticeably improved beyond that expected from the thermal figures of merit. Thus Fig. 2 can also be viewed as a relative measure of the effective interface heat transfer coefficient for the wheels examined.

The use of an iron substrate can be recommended for melt spinning amorphous products if the minimum or critical quench rate for that alloy system is not too high, such as for the AMS4778 and 4777 alloys. On the other hand, lower metalloid content alloys, such as the experimental low-boron AMS4778 alloy, have higher critical quench rates for amorphous state retention. Thus when melt spinning with an iron wheel, the nominal 20% reduction in interface heat transfer coefficient (extrapolated from Fig. 2) slows down the actual heat transfer rate sufficiently so that the amorphous state will not be fully retained. Even foils of this alloy melt spun on copper had an estimated crystalline content (Table V) in the 10 to 25% range, while the same alloy product melt spun on iron formed a fully crystalline foil.

Table V represents the results of a semiquantitative analysis for determining the crystalline/amorphous phase ratio. For this low boron alloy, foils melt spun on copper, iron and nickel- or chromium-electroplated copper wheels were examined by X-ray diffraction techniques. Using monochromatic Cu$K\alpha$ radiation, diffraction traces between 60° and 20° 2θ were recorded. Quantitative values were based on measurements of the integrated area $A(1\,1\,1)$ under the (1 1 1) fcc peak for the nickel-base solid solution phase (taken above the background radiation level or above the amorphous hump profile) as well as the integrated area $A(a)$ of the first diffuse amorphous hump above the background radiation level. Two ratios were calculated. One, the normalized $A(1\,1\,1)$ value compared to a reasonable but arbitrary value of 2100 (counts °2θ for a 100% crystalline standard sample), was the more direct method. However, it was subject to sample-to-sample and random equipment variations (estimated at up to ±20%; note that for the two different samples that were judged to be 100% crystalline, the $A(1\,1\,1)$ integrated areas were 2443 and 1851). The second method is more internally self-consistent as it ratios $A(1\,1\,1)$ against the sum of $A(1\,1\,1)$ and $A(a)$, making this term independent of instrumental or sampling errors. However, it is most likely that this ratio may underestimate the magnitude of the per cent crystallinity ratio, especially when the sample has very little crystalline phase and the measured value of $A(1\,1\,1)$ is quite small. For our purposes, the value for estimated per cent crystallinity was taken from the weighted average of both terms.

What should also be noted for this low boron AMS4778 foil melt-spun on the copper wheel is that there were significant differences in the degree of crystallinity on the free and contact surfaces. One rationalization is that the surface layer of the foil adjacent to the substrate must be exposed to temperatures between the "solidification" and the crystallization values for a proportionately longer period of time, while the rest of the overlaying elements, especially the free surface layer, solidify. Thus there is slightly more time for *in situ* crystallization to occur on the contact surface, especially when the critical quench rates are relatively higher than the easy-to-melt-spin alloys that form amorphous foils. Because the rest of the results in Table V were obtained from

the free surface side, the listed values, particularly for the foil made on the nickel-electroplated wheel, would represent a lower bound estimate of the actual amount of crystalline phase present; thus for this alloy only a copper wheel should be used if substantially amorphous materials are required.

4. Conclusions

This experimental programme has investigated the dynamic phenomenology of melt spinning in order to understand the effects that substrate and melt material composition have on melt puddle and product characteristics. In doing so, a statistically significant number of quantitative measures of the melt puddle shape and dimensions were taken over periods of time where steady-state conditions could be reached, at least in the case when a water-cooled copper substrate was used.

Evaluation of results shows that although melt spinning is a steady-state process where the type of substrate used can affect puddle features, significant product dimensions such as foil thickness are primarily controlled by process parameters. Specifically for foil thickness this value is inversely proportional to the translational velocity of the substrate [2, 6, 8–16, 44]. The complex, nonequilibrium nature of the dynamic melt/substrate interaction also makes it difficult to isolate how intrinsic substrate material properties such as metallic surface tension and bulk thermal transport properties (Table II) directly influence puddle characteristics, especially as these terms are respectively more appropriately applied to isothermal wetting and bulk heat flow dominated phenomena.

However, the observed systematic differences in puddle features as a function of substrate materials (Table III and Fig. 1) in each experiment represent phenomenological adjustments to the acting solidification kinetics. Mechanistically any substrate-related changes in the bulk thermal transport properties (due to the use of a substrate wheel other than copper) or the formation of an intermediate interface film can effectively lower the specific interface heat transfer coefficient appropriate to that melt spinning setup. This in turn forces puddle elongation so that the area magnitude of the heat transfer interface increases sufficiently such that the net integrated heat transfer rate needed to complete solidification at the preset melt introduction rate will remain nominally the same as that of a dressed copper wheel. It also appears that to preserve the puddle volume (as represented by the longitudinal cross-section $h \times l$ "area" term) there is a proportional decrease in puddle height and aspect ratio for the slower heat transfer substrate wheels.

Our results still indicate that copper is the best substrate material for nickel-base alloys, especially if the critical cooling rate to retain an amorphous structure is relatively high. An additional benefit is that a melt puddle on the copper wheel tends to be more compact and oscillate less; this in turn improves the dimensional uniformity of the product. The use of copper electroplated with nickel or a solid iron wheel is acceptable whenever the critical cooling rate to retain an amorphous foil from a given melt is not too high or when microcrystalline or crystalline products are desired. Also, in special cases when longer foil/wheel contact arcs are desired and if the melt contains some iron solute, this may be accomplished using an iron wheel.

While neither solid iron or copper electroplated with nickel can match the bulk thermal transport properties of copper, very good wheel interface contact with the solidifying foil occurs. Thus significant heat transfer rates can occur because the per cent effective contact area is very high. For chromium-plated copper and aluminium wheels, experimental results and foil quality are less than expected. In part this has been attributed to the formation of a tenacious oxide film that decreases the tendency of the wheel peripheral surface to be wetted by the melt. Macroexaminations of contact surfaces of foils melt spun from aluminium- or chromium-plated wheels reveal that the relative surface density of interface voids is higher than when copper is used. The oxide film also acts as an additional thermal flow resistance barrier. Both factors reduce the bulk heat flow rate, which causes puddle length extension, as described previously. Reduced heat transfer rates and more extensive wetting of the higher surface energy molybdenum substrate by the melt produced the extended puddle length and contact surface porosity when a molybdenum wheel was used. When the higher mechanical properties of molybdenum or iron relative to copper are required, such substrates must be designed to have a superior internal coolant heat-absorption capacity to avoid a significant rise in baseline wheel temperature. Otherwise degradation of foil quality will occur during long-term melt-spinning production runs.

A semiqualitative X-ray diffraction technique developed during this study enables the characterization of the amorphous/crystalline state of melt-spun foils from a statistically significant large sampling volume. Especially in cases where the effective substrate heat transfer rate is nearly equal to or less than the melt materials' critical quench rate, microstructural differences between foils produced from various substrate wheels have been established.

Further, when progressive, long-term changes in the amorphous/crystalline ratio were detected, it was possible to track time-varying changes in the thermal process parameters of certain melt-spinning systems. Thus time-temperature limitations to the use of our presently configured molybdenum wheel were identified. In particular, after 14 sec melt-spinning run time with an "easy" glass-forming AMS4778 alloy at a mass flow rate of approximately 11 g sec^{-1}, it was detected that a continuous, partially crystalline product started to form. After this the remaining 25% of the product was spun as a discontinuous, fully crystalline foil.

Additional X-ray diffraction measurements demonstrated that the contact and free surface regions of these nickel-metalloid melt-spun foils may have differing amorphous/crystalline phase ratios. These effects are due to different temperature–time cooling trajectories to which each thickness region is exposed during rapid solidification, but are more obvious for

the "harder" glass-forming melt chemistries due to their higher critical quench rate values. However, the use of substrates with lower thermal transport properties than copper can also produce similar effects even with the "easier" class of glass-forming alloys. Similar X-ray reuslts for the iron-metalloid systems have been reported [47–50] but were not attributed to this differential through-thickness thermal transient effect model. Further work is still necessary, but with proper diagnostics it should be possible to quantitatively obtain critical quench rates of alloys using this approach.

Each of the two compositional subclasses of the four nickel-metalloid alloys used has basically similar melt puddle chracteristics. Only a secondary difference in melt puddle volume was found where the metalloid richer (B > 10 at %, B + Si > 20 at %) alloy puddle was about 20% larger than that for the two metalloid leaner alloys. On the other hand, significant parameters such as the puddle contact length and the foil/wheel contact distance depended more systematically on the specific substrate evaluated, rather than on the actual melt composition. Nevertheless, real differences in the crystalline/amorphous nature of the foils were found that depended on both alloy and substrate selection. Thus, because the generalized puddle solidification process was essentially similar for all melt/substrate combinations, we believe that all these foils were initially amorphous as solidified. However, subsequent differences in primary (i.e. cooling by conduction into the wheel) and secondary (i.e. convective cooling after the foil leaves the wheel) heat transfer rates in conjunction with the relatively higher critical cooling rates for the "leaner" alloys produce post-solidification crystallization (partial or complete). In contrast, the two metalloid richer alloys retain the amorphous structure because the actual cooling rate is faster than the corresponding but much lower critical cooling rates for these alloys. Additional examination of chemically similar alloys that may solidify directly into crystalline foils has been anticipated [4] and will be systematically compared in a subsequent report.

In overview, these variable substrate melt-spinning experiments have been useful in understanding the concurrent, but distinct, solidification and cooling phenomena that occur to produce rapidly solidified melt-spun foils. Specific concepts are subsequently summarized.

1. The conversion of a liquid stream into a continuous foil is more significantly influenced by process parameters than by material properties. Interfacial heat transfer is the rate-controlling factor during solidification where self-adjusting puddle dimensions maintain the integrated thermal flux rate at a level sufficient to convert all the melt into a solid foil.

2. The strong influence of mechanical forces and the possible formation of an intermediate film along the heat transfer interface of the substrate wheel make the resultant dynamic wetting phenomena very complicated. Thus application of concepts and material properties normally associated with classical isothermal wetting experiments cannot be directly used to predict dynamic wetting behaviour.

3. Experimental conditions and solid/solid bonding forces that govern the foil/wheel contact time and the release process were also evaluated. The common element proposal suggesting improved bonding when the same element appeared on both sides of the foil/wheel interface appears to be selective rather than general. For the case of the AMS4777 alloy melt spun on a chromium-plated wheel and for all the alloys melt spun on the nickel-plated wheel, there was no extended foil residence time relative to the copper wheel. Only for the AMS4777 alloy melt spun on a low carbon steel wheel was there a significant increase that fitted this common element model.

Foil release downstream of the melt puddle appears to be a thermally related effect associated with the rate that the local wheel surface temperature drops from its maximum back to the baseline value. Thermal diffusivity is such a measure of the bulk thermal conductivity rate. Thus the puddle-to-release-point distance was compared on a melt by melt basis. For all melts the data for copper as well as the nickel- and chromium-plated substrates were expected to behave similarly and were found to cluster around a low value which we measured as a 25 + 10° arc angle. The extended residence for two runs with either iron or molybdenum wheels also fits this model. Whether or not the specific mechanism for iron wheels can be unambiguously established, some empirical indications that it promotes better foil quality may be related to more primary cooling during extended wheel contact; this lowering of the foil temperature before the slower secondary cooling regime occurs, undoubtedly produces a less oxidized, more ductile product. This is probably the reason why some workers cite iron as the substrate material of preference for making iron- and nickel-base alloys.

4. Finally we must reiterate that rapid solidification processes such as melt spinning should not be arbitrarily assumed to produce thin section foils with uniform through-thickness microstructures. Because the quench-rate trajectories of a given incremental layer element are a function of its distance from the foil/substrate interface during the unidirectional primary conductive cooling phase, as well as the subsequent secondary convective cooling phase, in reality there are no uniform through-thickness cooling rates. When melt-spinning "easy" glass-forming alloys with a well cooled, rotating copper substrate, the critical cooling rate is typically well below the actual cooling rate. Thus, this class of atomistically sluggish melt materials become amorphous foils retaining microchemical and microstructural uniformity even though various layer elements experience different cooling paths. This caveat is more significant when equipment with lower thermal transport substrates is used or when the "harder to form into glassy alloy" (i.e. with higher critical quench rates) materials must be melt spun. Under these conditions, in all cases whenever or wherever the effective local cooling rate falls below the "higher" critical quench rate, crystalline

phases will nucleate and graded through-thickness microstructures will be produced.

Acknowledgements

This work was sponsored by the Office of Naval Research under Contract No. N00014-82-C-434. We are grateful to Dr D. Polk, ONR Scientific Officer, and Dr J. R. McColl, Technical Manager at GTE Laboratories, for their comments and discussions, and to N. Schauder and W. Allen for their technical contributions. Analytical support by M. Downey, G. Hamill and J. Mullins in X-ray diffraction is appreciated. The nickel-base alloys were provided by GTE Wesgo.

References

1. T. MASUMOTO, Proceedings of 4th International Conference on Rapidly Quenched Metals, Sendai, Japan 1981, edited by T. Masumoto and K. Susuki (The Japan Institute of Metals, 1982) p. 1.
2. H. JONES, *J. Mater. Sci.* **19** (1984) 1043.
3. R. P. I. ADLER and S. C. HSU, "Critical Dynamics for Rapid Solidification Processing", Annual Report to Office of Naval Research for Contract N0014-82-C-0434, GTE Laboratories Technical Report TR 83-815.1 (September 1983).
4. *Idem*, "Critical Dynamics for Rapid Solidification Processing", Final Report to Office of Naval Research for Contract N0014-82-C-0434, GTE Laboratories Technical Report TR 84-815.1 (August 1984).
5. R. B. POND, US Pat. 2825108, 4 March (1985).
6. S. KAVESH, "Metallic Glasses", edited by J. J. Gilman and H. J. Leamy, (American Society for Metals, Metals Park, Ohio, 1978) p. 36.
7. J. H. VINCENT, J. G. HERBERTSON, and H. A. DAVIES, *J. Mater. Sci. Lett.* **2** (1983) 88.
8. H. HILLMAN and H. R. HILZINGER, "Rapidly Quenched Materials III", Vol. I, Proceedings 3rd International Conference on Rapidly Quenched Metals, edited by B. Cantor (The Metals Society, 1978) p. 22.
9. D. PAVUNA, *J. Mater. Sci.* **16** (1981) 2419.
10. R. P. I. ADLER and S. C. HSU, "Rapidly Solidified Metastable Materials", edited by B. H. Kear and B. C. Giessen, (Elsevier, 1984) p. 119.
11. S. TOMITA and H. SUSUKI, *J. Jpn Inst. Metals* **48** (2) (1984) 202.
12. H. R. HILZINGER and S. HOCK, Proceedings of Conference on Metallic Glasses: Science and Technology, Vol. 1", edited by C. Hargitai, I. Bakonya and T. Kemeny, (Central Research Institute for Physics, Budapest, 1980) p. 71.
13. S. J. B. CHARTER, D. R. MOONEY, R. CHEESE and B. CANTOR, *J. Mater. Sci.* **15** (1980) 2658.
14. F. E. LUBORSKY, H. H. LIEBERMANN, and J. L. WALTER, "Proceedings of Conference on Metallic Glasses: Science and Technology, 1", edited by C. Hargitai, I. Bakonya and T. Kemeny (Central Research Institute for Physics, Budapest, 1980) p. 203.
15. H. H. LIEBERMANN, *Mater. Sci. Engng.* **49** (1981) 185.
16. *Idem, ibid.* **43** (1980) 203.
17. *Idem, IEEE Trans. Magn. Mag-15* **6** (1979) 1393.
18. J. L. WALTER, "Rapidly Quenched Materials, III", Vol. I, Proceedings 3rd International Conference on Rapidly Quenched Metals, edited by B. Cantor (The Metals Society, 1978) p. 30.
19. H. R. HILZINGER, K. KRUGER and S. HOCK, US Pat. 4386648 (7 June 1983).
20. F. E. LUBORSKY and H. H. LIEBERMANN, *Mater. Sci. Engng* **49** (1981) 257.
21. N. TSUYA and K. ARAI, US Pat. 4257830 (24 March 1981).
22. N. TSUYA and K. ARAI, US Pat. 4265682 (5 May, 1981).
23. K. ESASHI and H. MINIATONO, US Pat. 4337087 (29 June, 1982).
24. P. H. SHINGU, K. KOBAYASHI, R. SUSUKI and K. TAKESHITA, Proceedings of 4th International Conference on Rapidly Quenched Metals", Sendai, Japan, 1981, edited by T. Masumoto and K. Susuki (The Japan Institute of Metals, 1982) p. 570.
25. H. A. DAVIES, N. SHOHOJI and D. H. WARRINGTON, Proceedings 2nd International Conference on Rapid Solidication: Principles and Technologies, edited by R. Mehrabian, (Reston, Virginia, 1980) p. 153.
26. H. SHOHOJI, H. A. DAVIES, H. JONES and D. H. WARRINGTON, Proceedings of 4th International Conference on Rapidly Quenched Metals", Sendai, Japan, 1981, edited by T. Masumoto and K. Susuki (The Japan Institute of Metals, 1982) p. 1529.
27. T. K. GLASGOW, personal communication, NASA Lewis Research Center, Cleveland, Ohio (September 1984).
28. S. SHIMANUKI, H. YOSHINO and K. INOMATA, Proceedings of 4th International Conference on Rapidly Quenched Metals", Sendai, Japan, 1981, edited by T. Masumoto and K. Susuki (The Japan Institute of Metals, 1982) p. 15.
29. M. C. NARASIMHAN, US Pat. 4331739 (25 May, 1982).
30. H. FIEDLER, H. MAHLBACH and G. STEPHANI, *J. Mater. Sci.* **19** (1984) 3229.
31. R. C. O'HANDLEY and N. J. GRANT, "Rapidly Solidified Amorphous and Crystalline Alloys", Materials Research Society Symposium Proceedings Vol. 8, edited B. H. Kear, B. C. Giessen and M. Cohen (1982) p. 217.
32. M. HAGIWARA, A. INOUE, H. TOMIOKA and T. MASUMOTO, Proceedings of 4th International Conference on Rapidly Quenched Metals", Sendai, Japan, 1981, edited by T. Masumoto and K. Susuki (The Japan Institute of Metals, 1982) p. 115.
33. J. V. WOOD, "Chemistry and Physics of Rapidly Solidified Materials", edited by B. J. Berkowitz and R. O. Scattergood (The Metallurgical Society of AIME, 1982) p. 79.
34. A. BENDIJK, R. DELHEZ, L. KATGERMAN, T. H. DEKEIJSER, E. J. MITTENEIJER and N. M. VAN DER PERS, *J. Mater. Sci.* **15** (1980) 2803.
35. S. M. L. SASTRY, T. C. PENG, P. J. MESCHTER and J. E. O'NEIL, *J. Metals* (September 1983) 21.
36. S. H. WHANG and B. C. GIESSEN, Proceedings 3rd Conference on Rapid Solidification Processing: Principles and Technologies, edited by R. Mehrabian (Gaithersburg, Maryland, 1982) p. 439.
37. S. H. WHANG, *J. Metals* (April 1984) 34.
38. B. N. DAS and N. C. KOON, *Met. Trans. A* **14A** (1983) 933.
39. J. J. CROAT and J. F. HERBST, *J. Appl. Phys.* **53** (1982) 2294.
40. S. H. WHANG, Barnett Institute of Chemical Analysis and Materials Science, Northeastern University, Boston, Massachusetts, personal communication (December 1984).
41. A. BONDI, *Chem. Rev.* **52** (1953) 417.
42. R. J. KLEIN WASSINK, *J. Inst. Metals* **95** (1967) 38.
43. J. V. NAIDICH and J. N. CHURASHOV, *J. Mater. Sci.* **18** (1983) 2071.
44. R. P. I. ADLER, S. C. HSU and R. V. RAMAN, "Influence of Processing Parameters on Melt Spinning Dynamics", Proceedings of 1984 Vacuum Metallurgy Conference on "Specialty Metals Melting and Processing", Pittsburgh, Pennsylvania (June 1984).
45. R. P. I. ADLER and S. C. HSU, Proceedings 3rd Conference on Rapid Solidification Processing: Principles and Technologies, edited by R. Mehrabian (Gaithersburg, Maryland, 1982) p. 448.
46. F. DUFLOS and J. -F. STOHR, *J. Mater. Sci.* **17** (1982) 3641.
47. L. A. DAVIS, N. DECRISTOFARO, and C. H. SMITH, Proceedings of Conference on Metallic Glasses: Science and Technology, Vol. I, edited by C. Hargitai, I. Bakonya and T. Kemeny (Central Research Institute for Physics, Budapest, 1980) p. 1.

48. M. CHOI, D. M. PEASE, W. A. HINES, J. I. BUDNICK, G. H. HAYE and L. T. KABACOFF, *J. Appl. Phys.* **54** (7) (1983) 41.
49. J. C. FORD, W. A. HINES, J. I. BUDNICK, A. PAOLUZI, D. M. PEASE, L. T. KABACOFF and C. U. MODZELEWSKI, *ibid.* **53** (3) (1982) 2288.
50. C. ANTONIONE, L. BATTEZZATI and G. VENTURELLO, Proceedings of 4th International Conference on Rapidly Quenched Metals", Sendai, Japan, 1981, edited by T. Masumoto and K. Susuki (The Japan Institute of Metals, 1982) p. 679.

Received 27 March
and accepted 8 June 1987